Progress In Electromagnetics Research C, Vol. 99, 145–156, 2020

Design of a Miniaturized Multilayer Tunable Super Wideband BPF

Aditi Sengupta[1, *], Somdotta R. Choudhury[2], and Santanu Das[1]

Abstract—A miniaturized multilayer tunable super wideband (SWB) bandpass filter (BPF) is presented based on a microstrip structure. A pair of transmission lines is coupled with the aid of three defected ground structures (DGS) at the ground to improve the coupling and provide a bandpass response. One of the transmission lines is placed at the top plane of the upper layer, and the other transmission line is at the bottom plane of the lower layer with defected microstrip structures (DMS) to improve the return loss. Bandwidth can be tuned by properly selecting the resonator size. The circuit model for the microstrip resonator and mathematical analysis are given and studied. Finally, the proposed structure with three pole SWB filter is designed, simulated, fabricated, and the results are well vindicated by an exemplary circuit centered at 6.5 GHz with the measured fractional bandwidth (FBW) of 135%. The filter exhibits relatively flat group delay throughout the passband that varies in the range 0.25–0.35 ns. The size of the resonator is 13.67 mm × 17.58 mm × 3.2 mm.

1. INTRODUCTION

High performance, reduced size, low-cost bandpass filters having wide fractional bandwidth (FBW) are highly desirable in modern microwave wireless communication systems. Planar resonators have been developed and implemented for narrowband filter applications. Resonators with shorter inter-spacing are required to achieve higher couplings for a wideband filter, which is a challenge in fabrication. Many methods have been proposed to design various WB bandpass filters (BPF) using single-layer microstrip structures. A wideband BPF with open loop resonator and floating metal patch is reported in [1]. A dual-band BPF with a conventional step impedance resonator (SIR) with increased selectivity is discussed in [2] and [3], respectively. A multiband BPF with three modes using stub loaded resonators is presented in [4]. A tri-band BPF using a multi-stub loaded multi-mode resonator is reported in [5] where the three passbands are controlled by eight modes. Wider bandwidths require tighter coupling between conductors, and this is where multilayer structures offer significant benefits. Metallization on both sides of a suspended stripline substrate to achieve wide-band response is realized in [6]. Multilayer band-pass filters having resonators with different geometries (square-loop, hairpin, parallel coupled, etc.) are proposed in [7] and [8], respectively. In [9] a UWB filter with different feed lines is designed and tested with low insertion loss, good band rejection, high return loss, and small group delay variation. It is demonstrated that the band rejection can be improved by cascading multiple filters. A compact multilayer UWB filter using folded three parallel coupled lines in a defected ground structure is analyzed in [10]. The selectivity and upper stopband performances of a filter with multilayer nonuniform periodical structure are improved and presented in [11]. A multilayer dual-mode dual-band BPF with a pair of identical slotted-patch resonators is presented in [12] where the coupling coefficients between the two resonators in each passband can be controlled independently. A compact lowpass filter (LPF) to UWB bandpass filter (BPF) is introduced in [13] using a simple transformation based on

Received 28 November 2019, Accepted 22 January 2020, Scheduled 4 February 2020
* Corresponding author: Aditi Sengupta (itsmeaaditi@gmail.com).
[1] Department of Electronics & Telecommunication Engineering, Indian Institute of Engineering Science & Technology, Shibpur, Howrah-711103, India. [2] Department of Electronics & Telecommunication Engineering, Ramrao Adik Institute of Technology, D. Y. Patil University Campus, Navi Mumbai-400706, India.

J-inverter technique. A UWB response is achieved due to back-to-back construction of vialess vertical hybrid CPW/microstrip transitions in [14]. A six-pole WB BPF with a folded slotline structure and microstrip-to-microstrip equal ripple vertical transitions is presented in [15]. A quarter wavelength SIR is introduced with multilayer arrangement to provide single band BPF in [16]. A miniaturized balanced BPF using the LCP bonded PCB multilayer technology is presented in [17] with controllable fractional bandwidth.

The cross-coupling between resonators placed in different layers with miniaturized structure along with several advantages of WB BPF compared with a single layer structure and having the same frequency is most challenging.

In this paper, a pair of transmission lines with DMSs consisting of DGSs in the back-to-back format is studied, designed, and a two-port equivalent-circuit model is constructed. The coupling arrangements of the two feed lines are made through the modified ground plane which is sandwiched between two substrate layers. This modified ground plane not only provides a sufficient coupling coefficient but also determines the cutoff frequencies of the SWB BPF. The schematic diagram of this filter in a multilayer structure having dimensions is shown in Fig. 1.

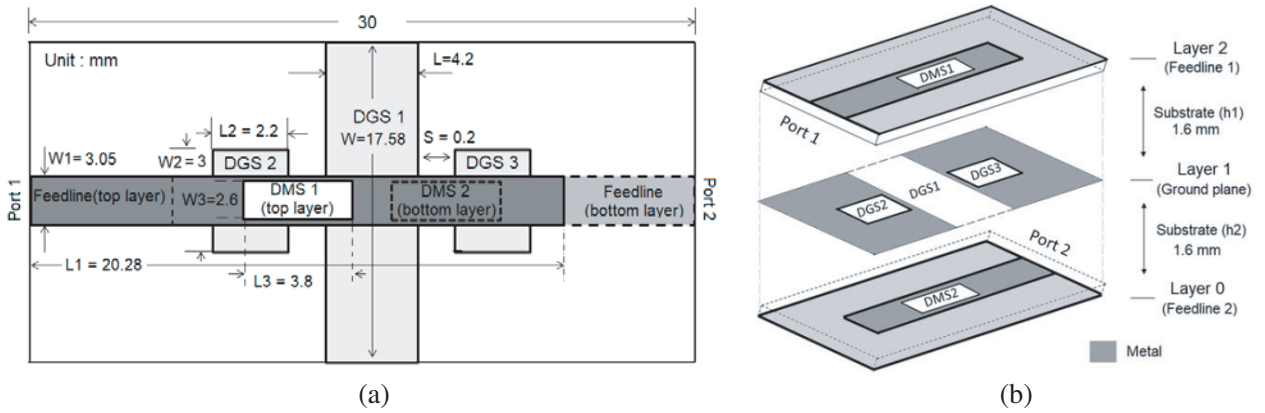

Figure 1. (a) Schematic diagram, (b) metallization layers of the proposed SWB-BPF: layer 2 (feedline 1), layer 1 (ground plane) and layer 0 (feedline 2).

Here the bandwidth is controlled by the physical dimension of the resonator. This compact filter is very useful in eliminating the disadvantages of conventional microstrip parallel-coupled line BPF with the advantage of a wide passband of 8.8 GHz (FBW = 135%). The center frequency of the filter is chosen as 6.5 GHz with cutoff frequencies at 2.14 GHz and 10.9 GHz. The insertion loss of the filter is quite low (0.4 dB) for this huge passband. Mathematical and parametric analysis is done to explain the filtering characteristic of the proposed SWB BPF. The structure is simulated and measured, and the responses show good matching between them.

This paper is organized as follows. Theoretical analysis of the WB BPF is discussed in Section 2 based on the proposed equivalent circuit. The parametric study of different parameters involved in the filter design is carried out in Section 3. The performance comparison of the proposed filter with a different dielectric substrate is discussed in Section 4. The comparison of simulation and measurement results of the filter is explained in Section 5 for validation. Section 6 concludes this paper.

2. THEORETICAL ANALYSIS

The SWB BPF shown in Fig. 1(a) is formed using two uniform transmission lines with two identical DMSs that are coupled through a common ground plane with DGSs in the multilayer of substrates in a different plane. The microstrip lines are connected with 50 Ω feedlines and are perpendicular to the DGS structures. A three-pole SWB is achieved in the form of stretching the electrical lengths by changing the size of open-circuited microstrip lines and DGS structures. Metallization layers of the proposed filter are shown in Fig. 1(b). Transmission lines are in the top layer (level 2) and bottom layer (level 0).

The middle layer (level 1) is a ground conductor and has defected ground to improve the coupling over a wide bandwidth. Coupled lines are quarter-wave long at the center frequency of the filter (6.5 GHz). DMS1, DMS2 and DGS2, DGS3 are identical and placed in different planes, respectively.

By representing the open-circuited microstrip line and DGS sections and assuming that all the discontinuities and losses can be neglected, a generalized transmission line model of a two-port equivalent circuit is developed in Fig. 2 to describe the proposed unit in Fig. 1. The coupled lines are described in terms of Kuroda identities having two series open-circuited stubs and a Unit Element (UE). The input impedance of the series open-circuited stubs is denoted here by Z_C; however, the characteristic impedance of unit element is taken as Z_U. The characteristic impedances representing the effect of both DGS and DMS sections are expressed in Z_D, assuming the same electrical length of θ_D, and the characteristic impedance of 50 Ω feedline is Z_0.

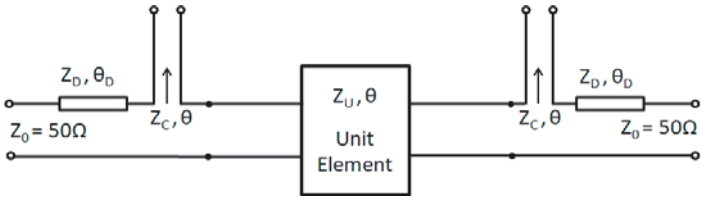

Figure 2. Equivalent transmission line model of the proposed filter.

The electrical parameters can be obtained based on derivations below from Equations (1)–(4). The whole ABCD matrix of the topology in Fig. 2 can be formulated as [15]:

$$M = \begin{bmatrix} \cos\theta + 2\dfrac{Z_C}{Z_U}\cot\theta\cos\theta & j\left(Z_U\sin\theta - 2Z_C\cot\theta\cos\theta\right) + Z_D\cos\theta \\ \dfrac{j}{Z_U}\sin\theta & \cos\theta \end{bmatrix} \tag{1}$$

where Z_D is considered as purely imaginary and given as,

$$Z_D = jX_D = 1\Big/\left(\frac{1}{j\omega L_D} + j\omega C_D\right) \tag{2}$$

where L_D and C_D are the effective inductive and capacitive reactance representing the effect of defected structures, respectively. The S-parameters of the proposed filter are given as

$$S_{11} = \frac{2Z_C\left(Y_U + jY_0\right)\cot\theta\cos\theta + j\left(Z_UY_0 - Y_UZ_0\right)\sin\theta + Z_DY_0\cos\theta}{\left(2 + Z_DY_0\right)\cos\theta + 2\left(Y_U + jY_0\right)Z_C\cot\theta\cos\theta + j\left(Z_UY_0 + Y_UZ_0\right)\sin\theta} \tag{3}$$

and

$$S_{21} = \frac{2}{\left(2 + Z_DY_0\right)\cos\theta + 2\left(Y_U + jY_0\right)Z_C\cot\theta\cos\theta + j\left(Z_UY_0 + Y_UZ_0\right)\sin\theta} \tag{4}$$

where $Y_U = 1/Z_U, Y_0 = 1/Z_0$.

Fig. 3 shows how differently S_{21} and S_{11} characteristics of the proposed filter change for various normalized values of Z_D. It shows that Z_D parameter in the equivalent circuit has a large effect on the S-parameter response of the filter. The change in Z_D is the result of a change in the physical dimension of DGSs and DMSs incorporated in the proposed structure i.e., $W = 14.58$ mm, $W = 15.58$ mm, $W = 16.58$ mm, $W = 17.58$ mm, $L_2 = 3.3$ mm, $L_2 = 1.1$ mm, and $L_3 = 5.8$ mm, respectively. It can be seen in the plot that as Z_D increases, the bandwidth of the filter decreases and vice versa. Z_C in the equivalent circuit is corresponding to the width of the coupled lines at the top and bottom planes. For this proposed structure, the coupled line width is taken as a fixed value which in turn causes a constant Z_C for this particular design. This Z_C certainly has a great effect on the response of the filter for a particular matching condition.

3. PARAMETRIC STUDY OF PROPOSED SWB BPF

Some of the physical parameters in the structure influence bandwidth and return loss of the filter. In this paper, an FR-4 epoxy substrate with a dielectric constant (ε_r) = 4.4 of thickness (h) = 1.6 mm and loss tangent (δ) = 0.02 is employed for the simulation and fabrication of the proposed transmission as described in Table 1.

Table 1. Geometrical parameters of band pass filter.

Substrate Thickness 'h_1' and 'h_2' Total $h = h_1 + h_2$	1.6 mm + 1.6 mm
Substrate permittivity 'ε_r'	4.4
Conductor thickness	10 µm
Number of layers	3

A parametric study is carried out to understand the effect of DGS length (L), coupling length (L_1) on bandwidth and the effect of DMS on return loss. To characterize the filter, some parameters of the filter structure are studied thoroughly. The corresponding s-parameter responses are shown in Fig. 4. The simulated response shows a super wideband bandpass response. Figs. 5–12 show the results of the parametric study.

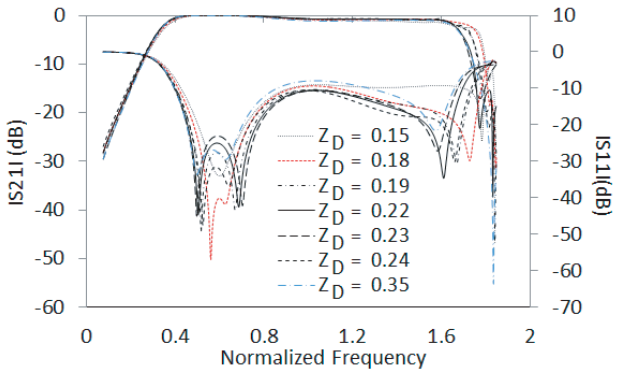

Figure 3. Normalized frequency responses of proposed SWB BPF with different values of Z_D.

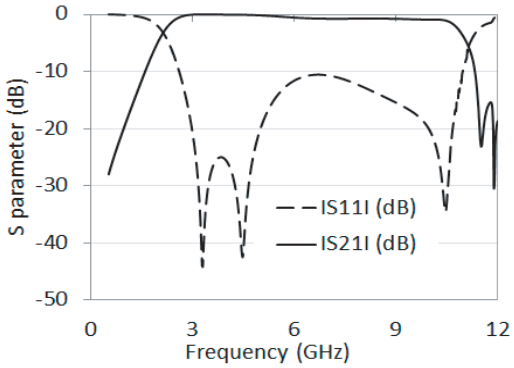

Figure 4. S-parameter response of the proposed filter.

There is a very minimal change in lower cutoff frequency due to the parameter's dimension change. To show the changes clearly in the upper sideband, some of the following Figs. 5–12 are presented with an inset diagram for insertion losses ($|S_{21}|$ dB).

3.1. Effect of Coupling Length

The change in length has significantly affected the bandwidth and return loss of the filter as shown in Figs. 5(a)–(b). The return loss diminishes with the increment of coupling length (L_1). The bandwidth is improved in the form of increasing upper cutoff frequency with decreasing value of length.

3.2. Effect of DMS Length

The S parameters are affected by the change of DMS length as shown in Figs. 6(a)–(b). With an increasing length (L_3), the return loss value diminishes. The insertion loss is controlled by DMS length, so proper value must be chosen for the length to get improved S_{21}.

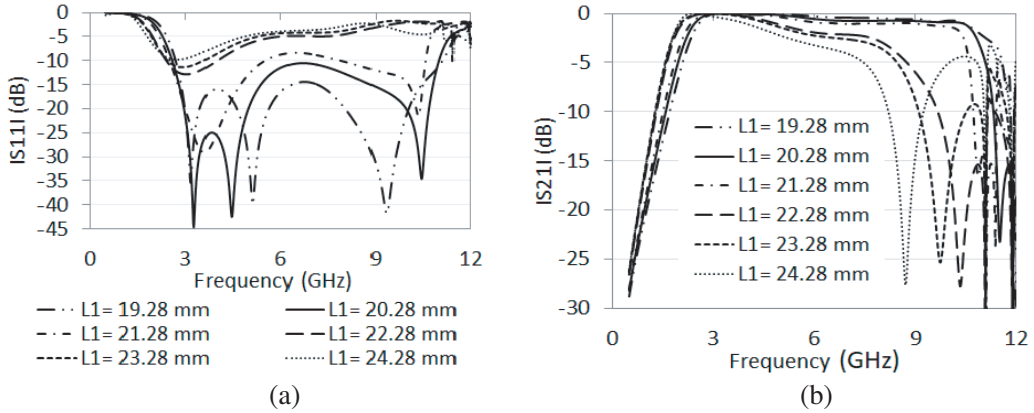

Figure 5. (a) Return loss response versus frequency, (b) insertion loss responses versus frequency for the change in coupling length (L_1).

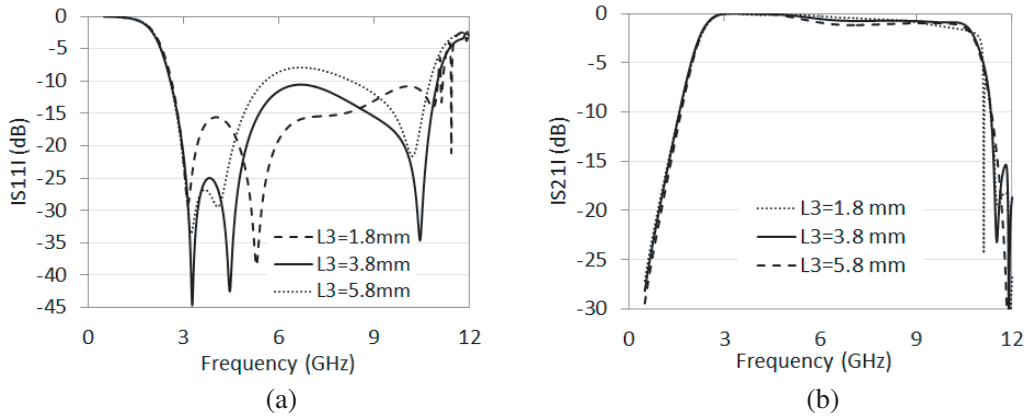

Figure 6. (a) Return loss response versus frequency, (b) insertion loss responses versus frequency for the change in DMS length (L_3).

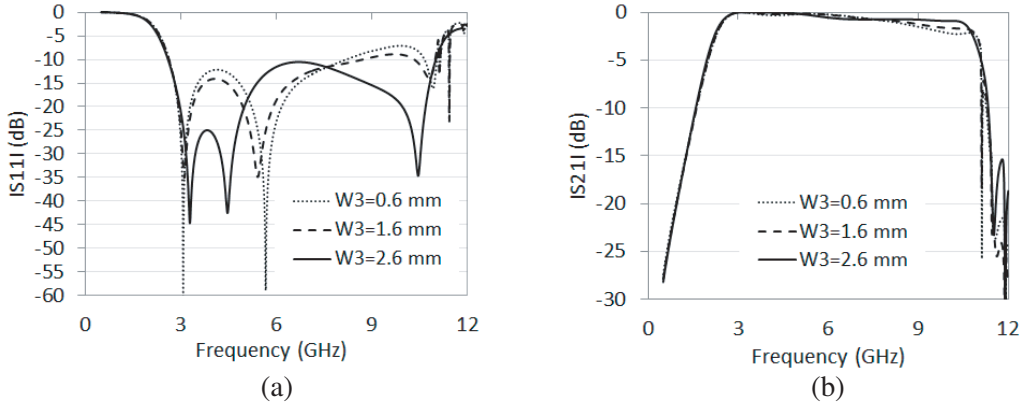

Figure 7. (a) Return loss response versus frequency, (b) insertion loss responses versus frequency for the change in DMS width (W_3).

3.3. Effect of DMS Width

The return loss and insertion loss both are improved with the increment of DMS width as shown in Figs. 7(a)–(b). A proper value of DMS width is chosen to get efficient results.

3.4. Effect of DGS2 Length

The effects of DGS2 length on S parameters are shown in Figs. 8(a)–(b). There is a very minimal change in return loss, and with the decrement of DGS2 length, the bandwidth is increased in terms of the upper cut-off frequency.

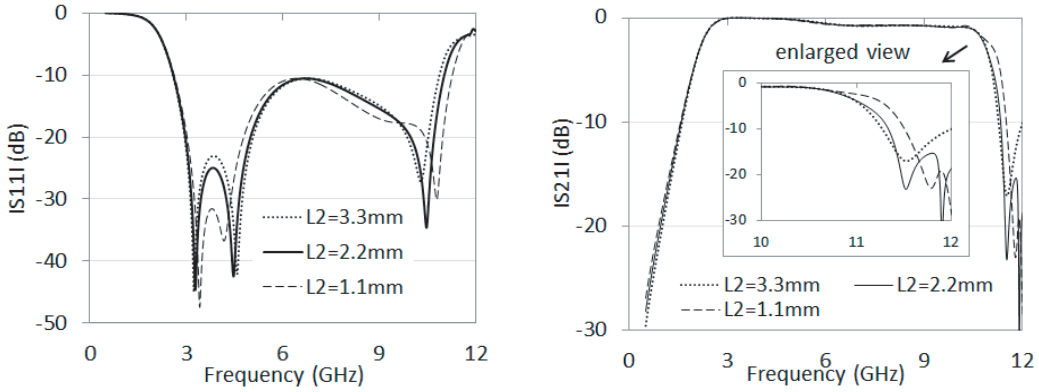

Figure 8. (a) Return loss response versus frequency, (b) insertion loss responses versus frequency for the change in DGS2-3 length (L_2).

3.5. Effect of DGS2 Width

The return loss and upper stopband rejection are improved due to DGS2 width increment as shown in Figs. 9(a)–(b).

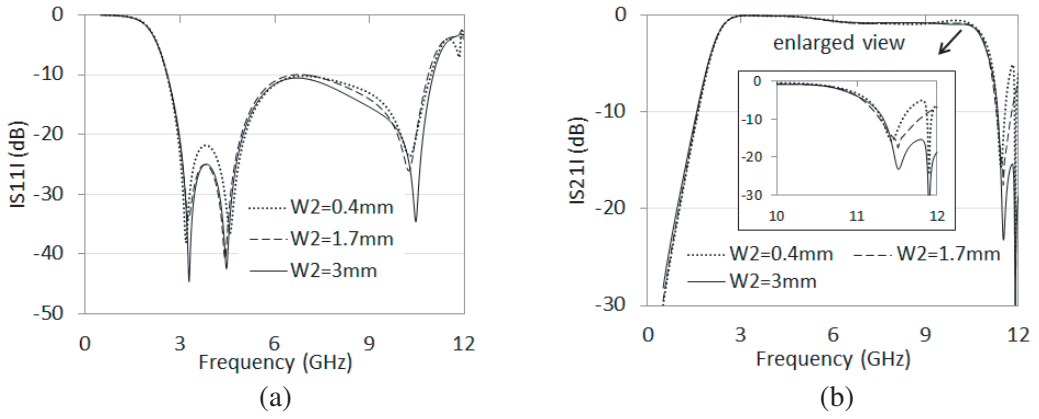

Figure 9. (a) Return loss response versus frequency, (b) insertion loss responses versus frequency for the change in DGS2-3 width (W_2).

3.6. Effect of DGS1 Length

Figures 10(a)–(b) show the change in S parameters due to DGS1 length change. The upper transition band and return loss are improved with the decrement of DGS1 length.

3.7. Effect of DGS1 Width

Here in Figs. 11(a)–(b), the return loss is improved, and upper stopband rejection is achieved with a good value due to the increment of DGS1 width. The bandwidth is increased in terms of the upper cutoff frequency with the decrement of DGS1 width (W).

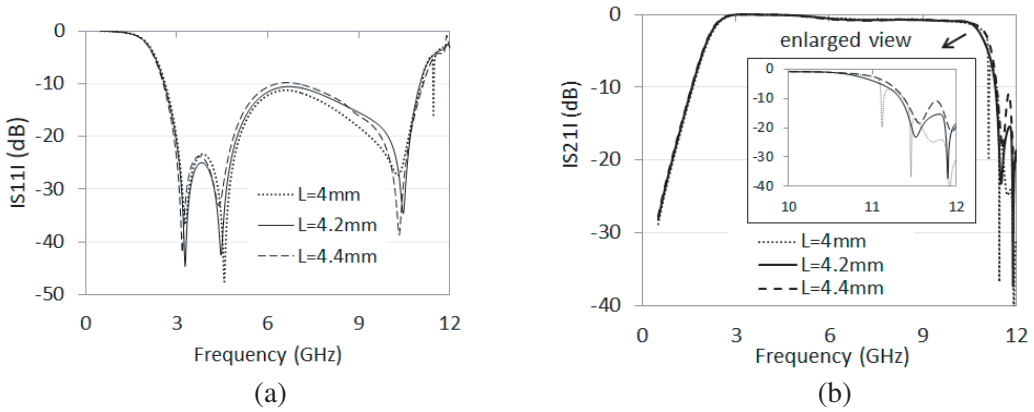

Figure 10. (a) Return loss response versus frequency, (b) insertion loss responses versus frequency for the change in DGS1 length (L).

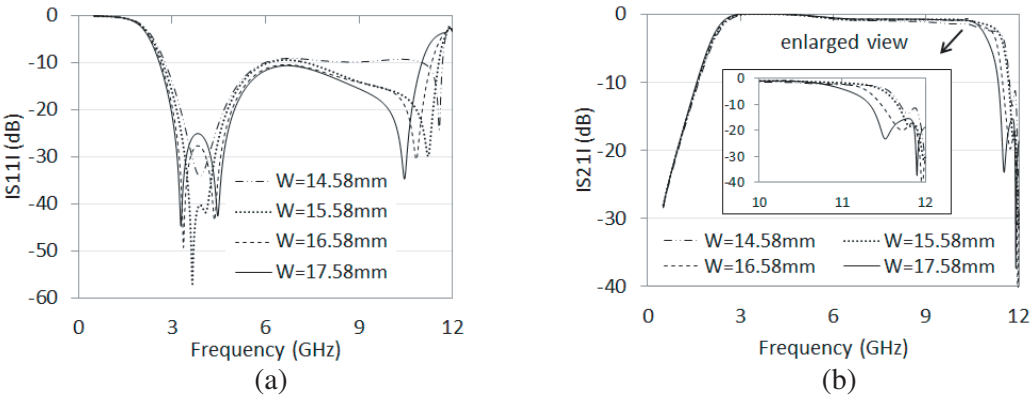

Figure 11. (a) Return loss response versus frequency, (b) insertion loss responses versus frequency for the change in DGS1 width (W).

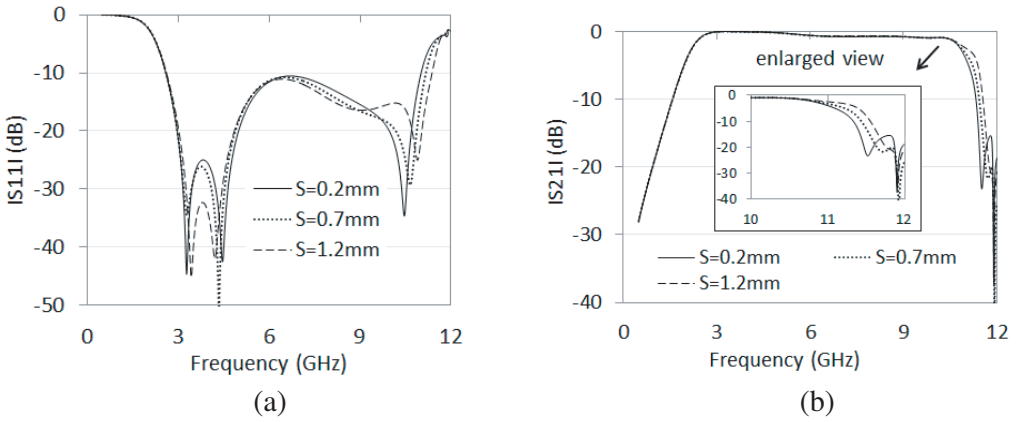

Figure 12. (a) Return loss response versus frequency, (b) insertion loss responses versus frequency for the change in spacing (S) between DGSs.

3.8. Effect of Spacing between DGSs

The spacing between DGSs plays an important role in determining the bandwidth of the filter as shown in Figs. 12(a)–(b). The bandwidth can be tuned in terms of the upper cutoff frequency with the change

in DGS spacing. The upper stopband rejection is improved with the decrement of spacing between DGSs.

So, the improvement of return loss is done by the change in coupling length (L_1), DMS length (L_3), and DMS width (W_3). Bandwidth can be tuned by the change in coupling length (L_1), DGS1 width (W), DGS2 length (L_2), and spacing (S) between DGSs. In this paper, L_1, W, L_2, and S are chosen to be 20.28 mm, 17.58 mm, 2.2 mm, and 0.2 mm, respectively, to achieve the required bandwidth. The proper values of L_3, W_3, and L_1 are chosen as 3.8 mm, 2.6 mm, and 20.28 mm, respectively, for improving the return loss. Comparing the results from the parametric study, the optimized dimensions of the SWB BPF are fabricated.

4. PERFORMANCE COMPARISON OF THIS FILTER USING A DIFFERENT DIELECTRIC SUBSTRATE

The performance of the structure presented here using an FR-4 epoxy substrate has been compared with the most similar designs of multilayer microstrip bandpass filters without DMS with an RT/Duroid 6010 substrate for microwave wireless communication systems. The substrate has a dielectric constant (ε_r) = 10.8, thickness (h) = 0.254 mm, and loss tangent (δ) = 0.0023. The basic design and metallization layers of the multilayer microstrip filter by an RT/Duroid 6010 substrate are shown in Fig. 13. The coupling arrangements of the two feed lines are made through the modified ground plane which is sandwiched between two substrate layers.

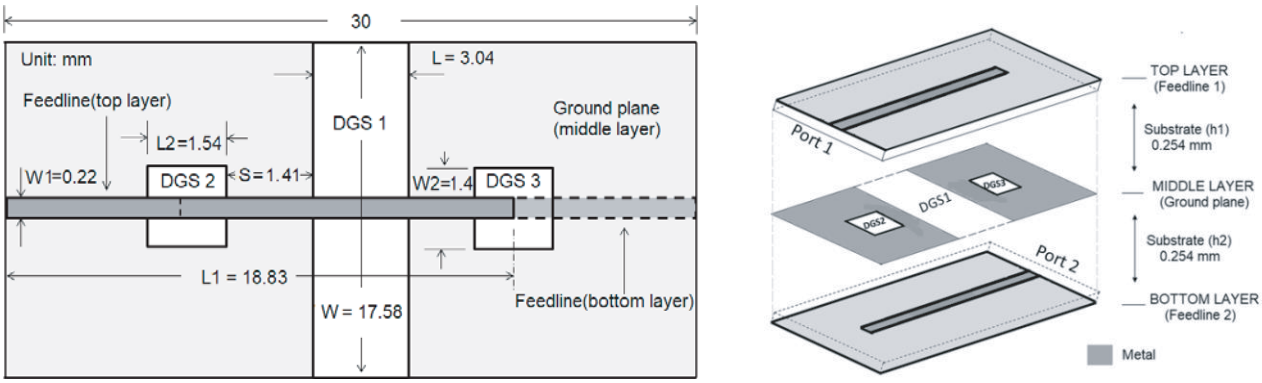

Figure 13. (a) Schematic diagram, (b) metallization layers of the BPF using RT/Duroid 6010 substrate.

The optimized dimensions of the microstrip bandpass filters are given in Table 2.

5. SIMULATION AND MEASUREMENTS

The simulated and measured frequency responses of the SWB BPF designed by an FR-4 epoxy substrate are displayed in Fig. 14(a). Full-wave simulation has been performed using Ansoft HFSS. The 3-dB passband of the filter covers the range of 2.14 GHz–10.9 GHz with the minimum return loss of 11 dB and maximum insertion loss of 0.4 dB. A prototype is measured using an Agilent N5230A network analyzer. The measured result agrees well with the simulated one. If the feed lines are ignored, the size of the resonator is $13.67 \times 17.58\,\text{mm}^2$ which amounts to $0.29\lambda_0 \times 0.3\lambda_0$ where λ_0 is the free-space wavelength of the operating frequency ($f_0 = 6.5$ GHz).

The simulated and measured group delays for the proposed filter are shown in Fig. 14(b). As seen from the figure, the group delay is relatively flat throughout the passband and varies in the range 0.25–0.35 ns. The reason for less group delay is the compactness of the structure. Constant group delay implies that all frequencies have the same phase and group velocity and therefore minimum frequency dispersion over the passband.

Table 2. Design dimensions of BPF.

Parameters	FR-4 epoxy (proposed SWB BPF)	RT/Duroid 6010
Coupling line width (W_1)	3.05 mm	0.22 mm
Coupling line length (L_1)	20.28 mm	18.83 mm
DGS 1 width (W)	17.58 mm	17.58 mm
DGS 1 length (L)	4.2 mm	3.04 mm
Spacing between DGS 1 and other DGSs (S)	0.2 mm	1.41 mm
DGS 2 and DGS 3 width (W_2)	3 mm	1.4 mm
DGS 2 and DGS 3 length (L_2)	2.2 mm	1.54 mm
DMS 1 and DMS 2 width (W_3)	2.6 mm	-
DMS 1 and DMS 2 length (L_3)	3.8 mm	-
Resonator size	13.67 mm × 17.58 mm	13.3 mm × 17.58 mm

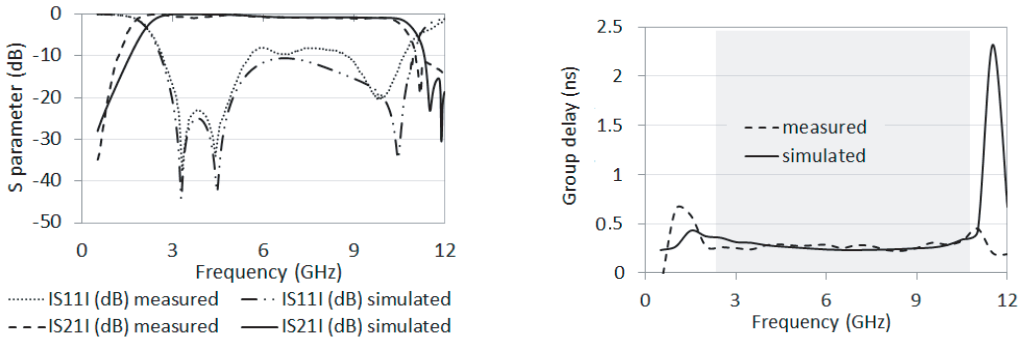

(a) (b)

Figure 14. The simulated and measured, (a) S parameter responses, (b) group delay responses of the proposed SWB BPF by Fr-4 substrate.

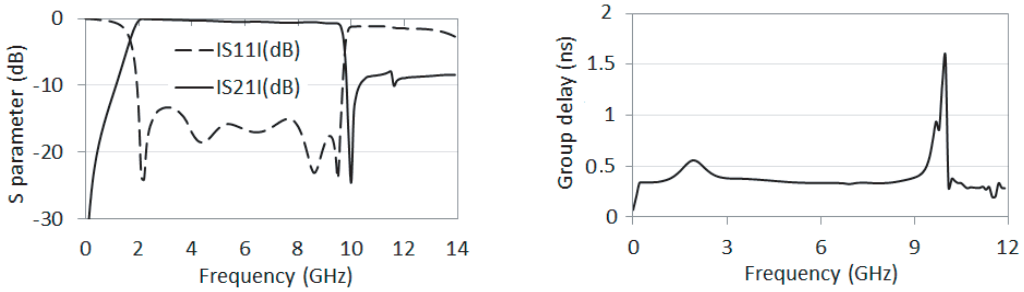

(a) (b)

Figure 15. The simulated, (a) S parameter responses, (b) group delay responses of microstrip BPF by RT/Duroid 6010 substrate.

Figure 15 illustrates the frequency response of microstrip BPF for the dielectric material RT/Duroid 6010, and it offers a WB response from 1.7 GHz to 9.6 GHz and a constant group delay of ±0.3 ns over the passband. The minimum return loss is 13.4 dB, and maximum insertion loss is 0.45 dB. The upper

Table 3. Performance comparison of microstrip BPF for different dielectric substrate.

Material/Substrate	$\|S_{11}\|$ dB	$\|S_{21}\|$ dB	**Bandwidth**	**FBW (%)**
FR4 epoxy	≥ 11	≤ 0.4	2.14 GHz–10.9 GHz	135
RT/Duroid 6010	≥ 13.4	≤ 0.45	1.7 GHz–9.6 GHz	139.8

Table 4. Comparison with other topologies.

Ref.	**PCB fabrication**	f_0 **(GHz)**	**size** ($\lambda_0 \times \lambda_0$)	**Dielectric constant/ height (mm)**	**Bandwidth**	**(−3 dB fractional bandwidth) FBW (%)**	$\|S_{21}\|$ dB	$\|S_{11}\|$ dB
[11]	3 layer	6.85	0.623 × 0.356	3.15/0.8	3.1 GHz–10.6 GHz	110	≤ 0.66	≥ 10
[14]	Single layer	6.85	0.3 × 0.27	10.2/0.635	1.68 GHz–10.06 GHz	141	≤ 0.85	≥ 15
[15]	3 layer	7.02	0.29 × 0.34	3.38/0.813	3.34 GHz–10.35 GHz	102	≤ 0.44	≥ 13.29
[17]	4 layer	6.85	0.436 × 0.26	3.0/0.5, 0.05, 0.1	2.9 GHz–10.9 GHz	118	≤ 1.1	≥ 12
This work	3 layer	6.5	0.29 × 0.3	4.4/1.6	2.14 GHz–10.9 GHz	135	≤ 0.4	≥ 11

stopband with an attenuation level better than 8.2 dB is up to 14 GHz. The upper transition band is only 0.3 GHz (from 9.6 GHz to 9.9 GHz). The full-wave simulation has been performed using Ansoft HFSS. If the feed lines are ignored, the size of the resonator is $13.3 \times 17.58\,\text{mm}^2$ which amounts to $0.25\lambda_0 \times 0.3\lambda_0$, where λ_0 is the free-space wavelength of the operating frequency ($f_0 = 5.6$ GHz).

It can be observed from Table 3 that the desirable substrate could be RT/Duroid 6010 which provides wider fractional bandwidth, improved return loss as compared to Fr-4 epoxy substrate, which is in low cost and easily available in the market.

Photographs of the top and middle layers of the proposed SWB BPF of FR-4 epoxy substrate are shown in Fig. 16(a); the top view of the assembled filter structure is shown in Fig. 16(b); and the setup of the measurement is shown in Fig. 16(c).

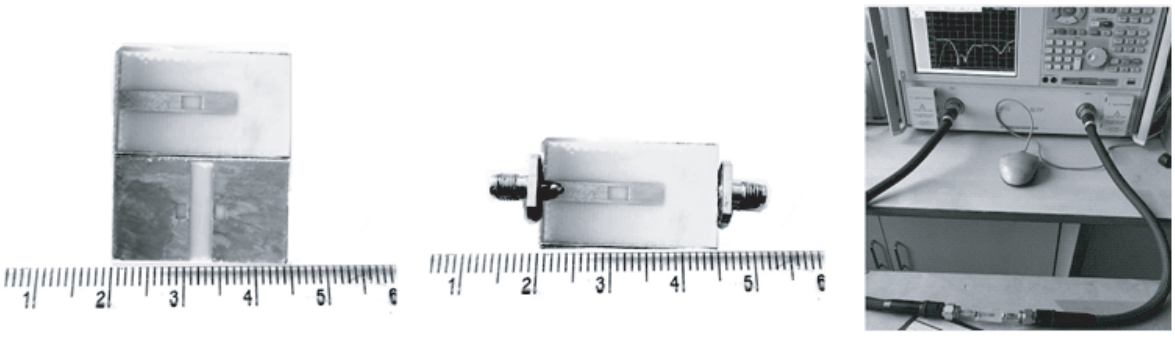

(a) (b) (c)

Figure 16. Photograph of the proposed SWB BPF of Fr-4 epoxy substrate: (a) view of top and middle layer, (b) top view of assembled filter, and (c) set-up of the measurement with results.

However, little discrepancy between simulated and measured ones may be attributed to fabrication tolerance and unexpected misalignment displacement during assembling process of two-layered substrates, and the measured filter with three pole SWB response is operated at 6 GHz (1.63–10.41 GHz) with the in-band maximum return loss of about 8.8 dB, and its fractional bandwidth is found about 140%.

Table 4 depicts the comparison of the present paper with reported works in terms of filter parameters and compactness of the filter. Taking λ_0 as the free-space wavelength operating at the center frequency (f_0), the resonator size is compared. The dimension of the proposed SWB BPF is of a competitive compact size, and the design structure is simpler than the existing works reported here. The proposed filter achieves good performances at higher frequencies and over a wider bandwidth. At the center frequency, the insertion loss is better than some referred journals reported here.

6. CONCLUSION

In this paper, a multilayer SWB BPF is constructed that includes a pair of transmission lines with DMSs consisting of DGSs on the common ground plane respectively in back-to-back format. The frequency responses are analyzed with an equivalent transmission-line model. The parametric analysis of different variables is carried out to obtain the optimized dimensions of the filter, and it is found that the return loss and bandwidth can be improved by changing the dimension of some specific parameters. The main advantage of the proposed filter is its miniaturized structure with a simple design that offers a wider frequency range of 2.14 GHz–10.9 GHz. The minimum return loss is 11 dB; maximum insertion loss is 0.4 dB; and its FBW is found about 135%. The filter exhibits relatively flat group delay throughout the passband that varies in the range 0.25–0.35 ns. To validate our proposed design method, good agreements between simulated and measured results are experimentally presented.

REFERENCES

1. Clavet, Y., E. Rius, C. Quendo, J. F. Favennec, C. Person, C. Laporte, C. Zanchi, P. Moroni, J. C. Cayrou, and J. L. Cazaux, "C-band multilayer bandpass filter using open-loop resonators with floating metallic patches," *IEEE Microw. Wirel. Compon. Lett.*, Vol. 17, No. 9, 646–648, September 2007.
2. Chang, W. S. and C. Y. Chang, "Analytical design of microstrip short circuit terminated stepped-impedance resonator dual-band filter," *IEEE Trans. Microw. Theory Tech.*, Vol. 59, No. 7, 1730–1739, July 2011.
3. García, R. G. and L. Yang, "Selectivity-enhancement technique for stepped-impedance-resonator dual-passband filters," *IEEE Microw. Wirel. Compon. Lett.*, Vol. 29, No. 7, 453–455, July 2019.
4. Chen, C. F., "Design of a compact microstrip quint-band filter based on the tri-mode stub-loaded stepped-impedance resonators," *IEEE Microw. Wirel. Compon. Lett.*, Vol. 22, No. 7, 357–359, July 2012.
5. Gao, L., X. Y. Zhang, and Q. Xue, "Compact tri-band bandpass filter using novel eight-mode resonator for 5G wifi application," *IEEE Microw. Wirel. Compon. Lett.*, Vol. 25, No. 10, 660–662, October 2015.
6. Schwab, W., F. Boegelsack, and W. Menzel, "Multilayer suspended stripline and coplanar line filters," *IEEE Trans. Microw. Theory Tech.*, Vol. 42, No. 7, 1403–1407, July 1994.
7. Hong, J. S. and M. J. Lancaster, "Aperture-coupled microstrip open-loop resonators and their applications to the design of Novel microstrip bandpass filter," *IEEE Trans. Microw. Theory Tech.*, Vol. 47, No. 9, 1848–1855, September 1999.
8. Djiaz, A. and T. A. Denidni, "A reduced-size two layer bandpass filter," *Microwave and Optical Technology Letters*, Vol. 44, No. 6, 512–515, February 2005.
9. Nedil, M., T. Denidni, A. Djaiz, and H. Boutayeb, "Ultra-wideband bandpass filters using multilayer slot coupled transitions," *Journal of Electromagnetic Waves and Applications*, Vol. 22, No. 4, 501–516, Taylor & Francis, 2008.

10. Packiaraj, D., K. J. Vinoy, and A. T. Kalghatgi, "Analysis and design of a compact multi-layer ultra wide band filter," *Progress In Electromagnetics Research C*, Vol. 7, 111–123, 2009.
11. Hao, Z. C., J. S. Hong, J. P. Parry, and D. P. Hand, "Ultra-wideband bandpass filter with multiple notch bands using nonuniform periodical slotted ground structure," *IEEE Trans. Microw. Theory Tech.*, Vol. 57, No. 12, 3080–3088, December 2009.
12. Chen, J. X., C. Shao, J. Shi, and Z. H. Bao, "Multilayer independently controllable dual band Bandpass filter using dual-mode slotted-patch resonator," *Electronics Letters*, Vol. 49 No. 9, 605–607, April 2013.
13. Boutejdar, A., M. Challal, A. A. Wael, A. Ibrahim, and P. Burte, "Compact LPF to UWB BPF transition employing quasi-triangular DGS resonators and a discontinuity on the microstrip feed line," *IEEE 4th International Conference on Electrical Engineering (ICEE)*, Boumerdes, Algeria, December 13–15, 2015, DOI: 10.1109/INTEE.2015.7416726.
14. Guo, Z. and T. Yang, "Novel compact ultra-wideband bandpass filter based on vialess vertical CPW/microstrip transitions," *Electronics Letters*, Vol. 53, No. 18, 1258–1260, August 2017.
15. Yang, L., L. Zhu, W. W. Choi, and K. W Tam, "Analysis and design of wideband microstrip-to-microstrip equal ripple vertical transitions and their application to bandpass filters," *IEEE Trans. Microw. Theory Tech.*, Vol. 65, No. 8, 2866–2877, August 2017.
16. Chen, J. X., Y. L. Li, W. Qin, Y. J. Yang, and Z. H. Bao, "Compact multilayer bandpass filter with wide stopband using selective feeding scheme," *IEEE Trans. Circuits Syst. II*, Vol. 65, No. 8, 1009–1013, August 2018.
17. Aliqab, K. and J. S. Hong, "UWB balanced BPF using a low-cost LCP bonded multilayer PCB technology," *IEEE Trans. Microw. Theory Tech.*, Vol. 67, No. 3, 1023–1029, March 2019.